

Exact results for the Kondo screening cloud of two helical liquids

Thore Posske,¹ Chao-Xing Liu,² Jan Carl Budich,¹ and Björn Trauzettel¹

¹*Institute for Theoretical Physics and Astrophysics,
University of Würzburg, 97074 Würzburg, Germany*

²*Department of Physics, The Pennsylvania State University,
University Park, Pennsylvania 16802-6300, USA*

We analyze the screening of a magnetic quantum dot with spin $\frac{1}{2}$ coupled to two helical liquids. Interestingly, we find two qualitatively different sets of Toulouse points, i.e., nontrivial parameters for which we can solve the two channel Kondo model exactly. This enables us to calculate the temperature and voltage dependent Kondo screening cloud, which develops oscillations for an applied spin voltage μ_s . Such a spin voltage can be conveniently applied by a charge bias in a four-terminal helical liquid setup.

PACS numbers: 72.10.Fk, 73.43.Nq, 75.76.+j

Introduction. The crucial ingredient of Kondo physics [1, 2] is the coupling of a localized spin degree of freedom, often represented by a spin on a quantum dot (QD), to a spin bath. In recent years, peculiarities relating to a plethora of realizations of the spin bath have been investigated [3–7]. One of the archetypal phenomena in Kondo physics which is still subject of active research is the characteristic screening of the QD-spin: while theorists predict a macroscopically extended screening which has been coined the Kondo cloud, experimental confirmation of this unique correlation is still lacking [8, 9]. Problems related to the direct detection of the Kondo cloud are the high frequency at which the spin of the QD is flipping and the principal inability to directly measure correlations between the QD-spin and the lead-spin without decisively perturbing the tunneling region. Helical liquids, which have recently been theoretically predicted [10–12] and experimentally discovered [13] at the edge of the quantum spin Hall insulator [10, 11, 14], feature two modes of excitations with opposite spins moving into opposite directions. The quantized conductance of $G = e^2/h$ of a single helical edge state is topologically protected against backscattering by time-reversal symmetry. A magnetic quantum dot coupled to helical liquids is one of the simplest nontrivial perturbations which allows elastic backscattering assisted by a spin flip of the QD [7]. Along these lines, former publications [7, 15] have mainly focused on the effect of a magnetic impurity on the conductance of the helical liquid and not on the screening of the localized spin. However, attaching helical liquids to a magnetic QD also offers unique opportunities to investigate spin-dependent scattering off the QD: by carrying away spin resolved information about the Kondo QD in distinct directions, correlations become measurable away from the QD avoiding the experimental necessity of locally perturbing the tunneling region.

We investigate an $S = \frac{1}{2}$ QD that is coupled to two helical liquids in a two channel Kondo model [16]. The relevance of this model is corroborated by a renormalization group study in Ref.[17]. In this Letter, we provide ex-

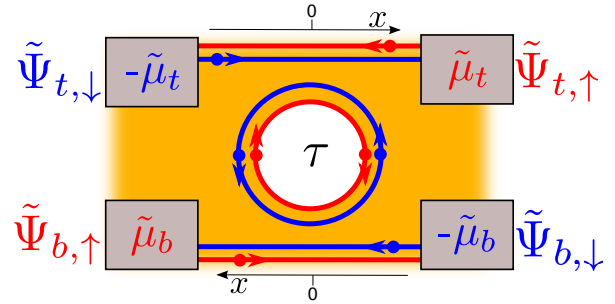


FIG. 1: (Color online) Two helical liquids of a quantum spin Hall insulator are coupled via an anti-dot. Properly gated, the dot resembles a magnetic impurity with $S = \frac{1}{2}$. Each side is brought out of equilibrium by an applied voltage.

act results for the local screening and the Kondo screening cloud. To this end, we solve the model by restricting the parameters to configurations for which an extension of the method of Emery and Kivelson [18] allows us to map the full interacting Hamiltonian to a quadratic one. We call these configurations Toulouse points following the terminology of the noninteracting case. Interestingly, we find two qualitatively distinct sets A and B of Toulouse points; set A contains the Toulouse point of the two channel Kondo model for noninteracting leads [18], while set B resembles a one channel Toulouse point at both Luttinger parameters $g = \frac{1}{2}$ [15]. Determining the local screening and the spatially extended Kondo screening cloud, we are able to demonstrate a different phenomenology for the novel interacting set of Toulouse points. For case A , the spin is always fully screened, however, case B , i.e. the interacting regime, provides the full range from no screening to exact screening. The Kondo cloud, defined as the correlations between QD-spin and lead-spin, obeys an asymptotic decay for large x that is quadratic at zero temperature. At finite temperature $T = 1/(k_B\beta)$, the decay becomes exponential after a length scale $\xi_T \approx \hbar v\beta$, which was also seen by Borda [8] for the one channel Kondo model. In contrast to the

noninteracting one channel case, we find a $\ln^2(x)$ instead of an x^{-1} divergence for small x . Furthermore, we observe that an applied spin flavor voltage $\mu_x = \tilde{\mu}_t + \tilde{\mu}_b$, whereby “flavor” denotes top(t) or bottom(b) (see Fig.1), and a spin voltage $\mu_s = \tilde{\mu}_t - \tilde{\mu}_b$ have distinct effects on the Kondo cloud. While the former acts as an artificial magnetic field which decreases the extent of the Kondo cloud significantly, the latter induces spatial oscillations of the Kondo cloud. Hence, the Kondo cloud can be easily manipulated in our four-terminal setup.

Model. A schematic setup is drawn in Fig.1 where the magnetic QD is realized by a properly gated anti-dot. Employing an anti-dot rather than a adatom in connection with helical liquids has the advantage that the anti-dot conserves the same pseudo spin, described in Refs.[19], as the helical liquids. This is important as the normal spin is not a good quantum number for experimentally realized helical liquids due to spin orbit coupling.

The modeling Hamiltonian is the two channel Kondo model for helical liquids, given by the sum of the three terms

$$\begin{aligned}\mathcal{H}_a &= \int dx \left(\sum_{\sigma \in \pm} v_{a,F} \tilde{\Psi}^\dagger(x)_{a,\sigma} (\sigma i \partial_x) \tilde{\Psi}(x)_{a,\sigma} \right. \\ &\quad \left. + \frac{g_{4,a}}{2} \tilde{\rho}_{a,\sigma}^2(x) + g_{2,a} \tilde{\rho}_{a,\downarrow}(x) \tilde{\rho}_{a,\uparrow}(x) \right), \\ \mathcal{H}_{KXY,a} &= J_a^\perp \tilde{\Psi}_{a,\uparrow}^\dagger(0) \tilde{\Psi}_{a,\downarrow}(0) \tau^- + H.c., \\ \mathcal{H}_{KZ,a} &= \frac{1}{2} J_a^z (\tilde{\rho}_{a,\uparrow}(0) - \tilde{\rho}_{a,\downarrow}(0)) \tau^z\end{aligned}\quad (1)$$

for each side $a \in \{t, b\}$. Here, the operators $\tilde{\Psi}_{a,\sigma}$ and τ represent the fermions of the leads and the spin of the QD respectively, $v_{a,F}$ is the Fermi velocity, the interaction strengths within the leads are denoted by $g_{2/4,a}$ and the coupling constants J_a^σ with $J_a^x = J_a^y \equiv J_a^\perp$ determine the strength of the coupling of the leads to the QD. Following Ref.[20], the helical liquids are bosonized using the bosonization identity $\tilde{\Psi}_{a,\sigma}(x) = \frac{1}{\sqrt{2\pi a}} F_{a,\sigma} e^{-i\tilde{\varphi}_{a,\sigma}(x)}$ and diagonalized by introducing the fields

$$\begin{aligned}\varphi_{a,\sigma}(x) &= \frac{1}{\sqrt{8}} \left[\frac{1+g_a}{\sqrt{g_a}} (\tilde{\varphi}_{a,\uparrow}(x) - \sigma \tilde{\varphi}_{a,\downarrow}(-x)) \right. \\ &\quad \left. + \frac{1-g_a}{\sqrt{g_a}} (\sigma \tilde{\varphi}_{a,\uparrow}(-x) - \tilde{\varphi}_{a,\downarrow}(x)) \right]\end{aligned}\quad (2)$$

with the Luttinger liquid parameters g_a and v_a , which depend on $v_{a,F}$ and $g_{2/4,a}$. This leads to

$$\begin{aligned}\mathcal{H}_a &= \int dx \frac{v_a}{2} \sum_{\sigma} (\partial_x \varphi_{a,\sigma}(x))^2, \\ \mathcal{H}_{KXY,a} &= \frac{1}{4\pi a} J_a^\perp F_{a\uparrow}^\dagger F_{a\downarrow} e^{(i\sqrt{2g_a}\varphi_{a,+}(0))} \tau^- + H.c., \\ \mathcal{H}_{KZ,a} &= \frac{1}{2} J_a^z \frac{\sqrt{2g_a}}{4\pi} \partial_x \varphi_{a\sigma}(0) \tau^z.\end{aligned}\quad (3)$$

	<i>A</i>	<i>B</i>
v_t	v	
v_b	v	
g_t	$2 \sin^2(q)$	$\sin^2(q)$
g_b	$2 \cos^2(q)$	$\cos^2(q)$
$g_t + g_b$	2	1
J_t^z	$2\pi v$	$2\pi v(1 \pm \cot q)$
J_b^z	$2\pi v$	$2\pi v(1 \pm \tan q)$

TABLE I: Toulouse points of the two channel Kondo model for helical liquids. There are two disconnected sets *A* and *B* of Toulouse points. The parametrization uses $v \in (0, \infty)$ and $q \in (0, \pi/2)$.

We furthermore include the chemical potentials $\tilde{\mu}_a$ by the nonequilibrium operator [15, 21]

$$\mathcal{Y} = \sum_{a \in \{t, b\}} \tilde{\mu}_a \left(\tilde{\mathcal{N}}_{a,\uparrow} - \tilde{\mathcal{N}}_{a,\downarrow} \right), \quad (4)$$

where $\tilde{\mathcal{N}}_{a,\sigma}$ is the total number operator of the fermion $\tilde{\Psi}_{a,\sigma}$. In principal, independent chemical potentials at each terminal depicted in Fig.1 could be considered. However, as the Kondo interaction is a spin interaction, the two potential configurations that are only able to alter charge densities are not relevant for the Kondo physics. Therefore, we do not consider them here.

Method. The aim is to find the Toulouse points of the Hamiltonian, i.e. points in the parameter space for which there is a mapping of the Hamiltonian from Eq.(3) to a quadratic one following the ideas of Refs.[18, 22, 23]: (i) applying an Emery-Kivelson rotation $U = \exp(i \sum_a \lambda_{a,+} \varphi_{a,+}(0) \tau^z)$, (ii) transforming $\varphi_{a,\pm}$ orthonormally to fields $\phi_j = \sum_{a,\sigma} M_{j,(a,\sigma)} \varphi_{a,\sigma}$, (iii) refermionizing. This technique has also been recently employed to analyze the Kondo problem for a single helical liquid in Ref.[24].

In our setup, we obtain all Toulouse points by restricting J_a^z to the value such that $\mathcal{H}_{KZ,a}$ cancels the Emery-Kivelson rotation of \mathcal{H}_a and secondly imposing that all vertex operators after step (ii) take a refermionizable form. Here we distinguish two possibilities. Within case *A* both vertex operators take the form $e^{\pm i\phi_4(0)}$, while for case *B* the form of one vertex operator deviates to $e^{\pm i\phi_2(0)}$, where ϕ_2 and ϕ_4 are linearly independent. A representation of all Toulouse points is given in Tab.I. Case *A* is characterized by $g_t + g_b = 2$ and contains the noninteracting case. In contrast, the novel case *B* obeys $g_t + g_b = 1$ and intrinsically relies on interactions. In particular, it contains $g_t = g_b = \frac{1}{2}$ for which refermionization is known to be a promising method in similar models [15, 20] and possesses two solvable values of $J_{t/b}^z$ for each solvable configuration of $g_{t/b}$.

The grand canonical operators of the resulting reso-

nant level models are [18]

$$\mathcal{H}_A = -\mu_x \mathcal{N}_2 - \mu_s \mathcal{N}_4 + \mathcal{H}_0 + \frac{1}{2\sqrt{2\pi a}} \left(J_L^\perp \Psi_4^\dagger(0)c + J_R^\perp \Psi_4(0)c + H.c. \right) \quad (5)$$

with the local pseudofermion $c = G_2^\dagger \tau^-$, for case A , and

$$\mathcal{H}_B = -(\mu_x - \mu_s) \mathcal{N}_2 - (\mu_x + \mu_s) \mathcal{N}_4 + \mathcal{H}_0 + \frac{1}{2\sqrt{2\pi a}} \left(J_L^\perp \Psi_4^\dagger(0)c + J_R^\perp \Psi_2^\dagger(0)c + H.c. \right). \quad (6)$$

with $c = \tau^-$ for case B . The fermions are determined by $\Psi_j(x) = \frac{1}{\sqrt{2\pi a}} G_j e^{-i\phi_j(x)}$, where we exploited the treatment of Klein factors G_j and number operators \mathcal{N}_j in Refs.[20, 23] for the cases A and B , respectively. In both cases, the noninteracting Hamiltonian is given by $\mathcal{H}_0 = v \sum_j \int dx \Psi_j(x) (-i\partial_x) \Psi_j(x)$. The main difference between the Hamiltonians is the absence of double creation terms in \mathcal{H}_B . In particular, \mathcal{H}_B shows no signs of Majorana fermions, which are central in the treatment of \mathcal{H}_A [18]. This is a direct consequence of the introduction of two linearly independent fermionic fields in case B . Interestingly, for both cases, the dependence on the Luttinger parameters on both sides is excluded from the Hamiltonian and incorporated in the transformation between the original fermions $\tilde{\Psi}_\alpha$ and Ψ_α . As will be seen below, this gives rise to simple algebraic relations between observables at different Toulouse points.

The Hamiltonians of Eqs.(5) and (6) are solvable via a variety of techniques, see, e.g. Refs.[21, 23]. Our results are based on infinite order perturbation theory in the Keldysh formalism. Conveniently, we exploit a treatment introduced in Ref.[15] and replace the voltage μ_x by an artificial magnetic field H_{art} at the QD for the Hamiltonian of Eq.(5)

$$-\mu_x \mathcal{N}_2 \rightarrow \mu_x c^\dagger c =: H_{\text{art}} \mu_B g_{\text{QD}} (\tau^z + \frac{1}{2}) \quad (7)$$

with $H_{\text{art}} = \mu_x / (\mu_B g_{\text{QD}})$. This substitution leaves all thermodynamic expectation values considered in this paper invariant and has an appealingly simple physical foundation given in Ref.[15]. Notably, for a Landé factor g_{QD} on the order of 10, a spin flavor voltage of 1V generates an artificial magnetic field on the order of $10^3 T$.

Results. We focus now on the z -screening of the spin τ of the QD. The contributions to this quantity are the local screening at $x = 0$, determined by the locally bound spin in the leads, and the spatially extended Kondo cloud. The local screening S_0^z is given by

$$S_0^z = \sum_a \int_{-\epsilon}^{\epsilon} dx \langle \tilde{\rho}_{\text{spin},a}^z(x) \rangle = -\langle \tau^z \rangle \begin{cases} 1 & A \\ \frac{1}{2} \mp \sqrt{g_t g_b} & B \end{cases} \quad (8)$$

with $\tilde{\rho}_{\text{spin},a} = \frac{1}{2}(\tilde{\rho}_{a,\uparrow} - \tilde{\rho}_{a,\downarrow})$, $\epsilon = 0^+$, and the “ \mp ”-sign corresponds to the two possible branches of Toulouse points in case B described in Tab.I. Hence, for all Toulouse points of case A the spin is locally exactly screened, case B however provides Toulouse points ranging from zero to exact screening. Both extremes appear for $g_t = g_b = \frac{1}{2}$ for which $J_t^z = J_b^z \equiv J^z$. At this Toulouse point, the local screening is more meaningfully described in the form $S_0^z = -J^z / (4\pi v) \langle \tau^z \rangle$. Consequently, the local screening vanishes for the Toulouse point with $J^z = 0$ and reaches exact screening for $J^z = 4\pi v$.

The Kondo screening cloud $\chi_a^z(x)$ is represented by the spatially resolved correlations between the QD-spin and the lead-spin [25]

$$\chi_a^z(x, g_{t,b}) = \langle \delta \tilde{\rho}_{\text{spin},a}(x) \delta \tau^z \rangle, \quad (9)$$

with $\delta A = A - \langle A \rangle$. We find that in our case, all Kondo clouds are derivable from two generic Kondo clouds. One stems from the noninteracting Toulouse point in case A and the other from the $g_t = g_b = \frac{1}{2}$ Toulouse point in case B . We denote them by $\chi_a^z(x, 1)$ and $\chi_a^z(x, \frac{1}{2})$ respectively. For case A , the general Kondo cloud is related to the noninteracting one by

$$\chi_a^z(x, g_{t,b}) = g_a \chi_a^z(x, 1) \quad (10)$$

with $a \in \{t, b\}$. Furthermore, the sum rule

$$\frac{1}{g_t} \chi_t^z(x, g_{t,b}) + \frac{1}{g_b} \chi_b^z(x, g_{t,b}) = 0. \quad (11)$$

connects the Kondo clouds of both sides. In combination, Eqs.(11) and (10) imply that there is no Kondo cloud in case A if $J_t^\perp = J_b^\perp$, i.e. in the case of symmetric coupling. Interestingly, Eq.(11) also shows that the Kondo correlations of different sides have different signs. Thereby, the side of positive correlations is determined by the weaker in plane coupling $|J_a^\perp|$.

Similarly, for case B , the Kondo clouds for different Luttinger parameters are related by

$$\chi_b^z(x, g_{t,b}) = \sqrt{g_b} ((\sqrt{g_b} - \sqrt{g_t}) \chi_t^z(x, \frac{1}{2}) + (\sqrt{g_b} + \sqrt{g_t}) \chi_b^z(x, \frac{1}{2})), \quad (12)$$

and the Kondo cloud on the t -side follows by exchanging $b \leftrightarrow t$ in the above formula. A direct consequence of Eq.(12) is the independence of the total Kondo cloud on the Luttinger parameters of both sides

$$\chi_t^z(x, g_{t,b}) + \chi_b^z(x, g_{t,b}) = \chi_t^z(x, \frac{1}{2}) + \chi_b^z(x, \frac{1}{2}). \quad (13)$$

In equilibrium, the analytic expressions for the generic Kondo clouds read

$$\chi_t^z(x, 1) = \text{sgn}(J_b^\perp - J_t^\perp) \frac{k_B \sqrt{T_1^K T_2^K}}{4\pi^2 v} e^{-\frac{2\pi x}{\hbar v \beta}} \tilde{\Phi}(x, \beta, T_1^K) \tilde{\Phi}(x, \beta, T_2^K), \quad (14)$$

$$\chi_t^z(x, \frac{1}{2}) = \frac{k_B T_t^K}{4\pi^2 v} e^{-\frac{2\pi x}{\hbar v \beta}} \tilde{\Phi}^2(x, \beta, T_1^K + T_2^K), \quad (15)$$

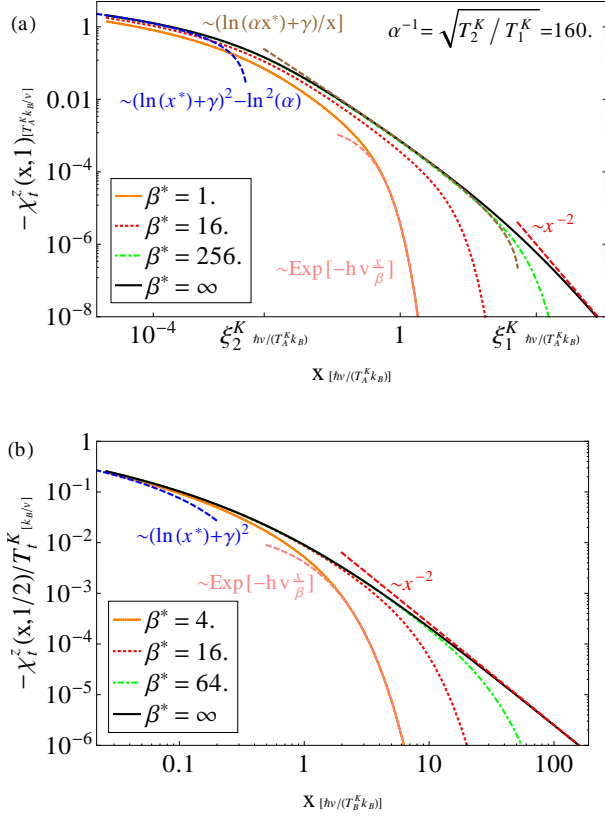


FIG. 2: (Color online) The decay of the generic Kondo clouds in equilibrium for different inverse temperatures $\beta^* = k_B T_{A/B}^K \beta$ on a double-logarithmic scale. For finite temperature, the Kondo cloud decays exponentially after a length scale $\xi_T \approx \hbar v \beta$. The relevant limits of the cloud are depicted as dashed curves, γ is the Euler-Mascheroni constant. (a) Noninteracting Kondo cloud. The temperature of reference is T_A^K . Both Kondo temperatures $T_{1/2}^K = \hbar v / (k_B T_{1/2}^K)$. (b) Interacting Kondo cloud rescaled by T_t^K . The temperature of reference is T_B^K . The curve is universal for all J_a^\perp and only the length scale determined by T_B^K is relevant.

where $\tilde{\Phi}(x, \beta, T^K) = \Phi(e^{-\frac{2\pi x}{\hbar v \beta}}, 1, \frac{1}{2} + \frac{1}{2\pi} \beta k_B T^K)$ with the Hurwitz-Lerch transcendent $\Phi(z, s, \alpha) = \sum_{n=0}^{\infty} \frac{z^n}{(n+\alpha)^s}$, $T_{1/2}^K = \frac{(J_a^\perp \mp J_b^\perp)^2 \hbar}{16\pi a k_B v}$ are the Kondo temperatures of our system [21] and $T_t^K = \frac{(J_a^\perp)^2 \hbar}{16\pi k_B v a}$. The equilibrium Kondo cloud is shown in Fig.2. Concerning case A, given in Fig.2(a), we chose $T_A^K = \sqrt{T_1^K T_2^K}$ to be the temperature of reference. Both Kondo length scales $\xi_{1/2}^K = \hbar v / (k_B T_{1/2}^K)$ appear in the shape of the Kondo cloud by inducing a crossover to different asymptotic behaviors. The leading divergence for small x is $\ln^2(x)$ and the asymptotic behavior for large x is a quadratic decay. For finite temperature the Kondo cloud decays exponentially in x after a length scale $\xi_T \approx \hbar v \beta$ similar to Ref.[8].

For case B, the temperature of reference is conveniently chosen to be $T_B^K = T_1^K + T_2^K$. Rescaled by T_t^K ,

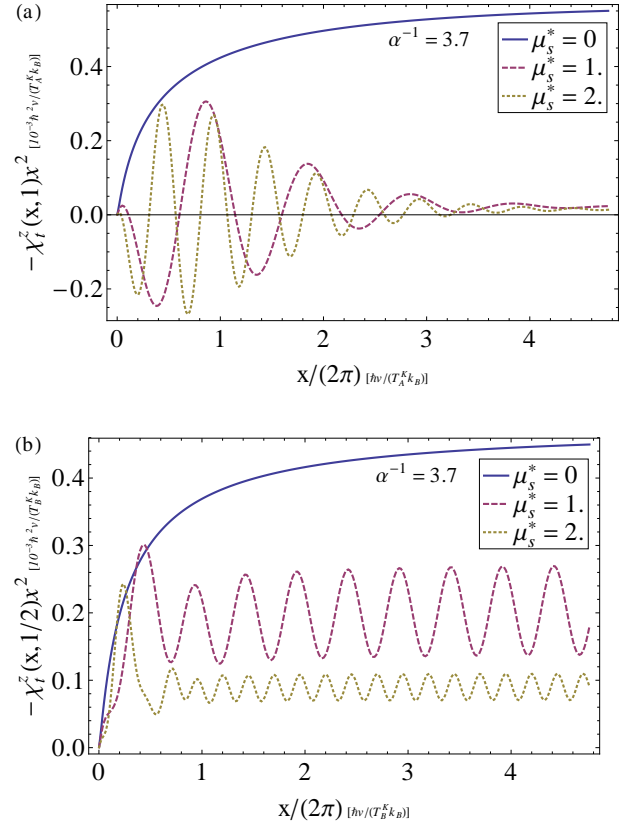


FIG. 3: (Color online) The generic Kondo clouds rescaled by x^2 at zero temperature in nonequilibrium. (a) Noninteracting Kondo cloud. An applied spin voltage $\mu_s = k_B T_{A/B}^K \mu_s^*$ induces exponentially decaying oscillations of the frequency $\mu_s / (\hbar v)$ in the Kondo cloud and locally changes its sign. (b) Interacting Kondo cloud. Additional permanent oscillations of the frequency $2\mu_s / (\hbar v)$ appear.

the generic Kondo cloud of side t is a universal curve for all coupling parameters. In contrast to case A, the only relevant length scale is determined by $\xi_B^K = \hbar v / (k_B T_B^K)$. The asymptotic behavior of the depicted curves in Fig.2 coincides in the large x limit and differs only by the constant $\ln^2(T_1^K / T_2^K) / (4\pi)^2$ for small x . For $T_1^K = T_2^K$, they become equivalent.

Applied voltages μ_x and μ_s alter the Kondo cloud distinctly. The spin flavor voltage μ_x acts as a magnetic field and strongly shrinks the Kondo cloud in both classes of Toulouse points. This reflects the sensitivity of Kondo physics to unhindered spin flips of the QD. An increasing μ_s instead induces oscillations in the Kondo cloud depicted in Fig.3. For case A, an oscillation of the frequency $\mu_s / (\hbar v)$ changes the sign of the Kondo cloud locally. This oscillation decays exponentially and the Kondo cloud becomes monotonic again for large x . For case B, the universality of the Kondo cloud at a specific T_B^K is destroyed. In addition to the known oscillations of case A, case B shows oscillations of the frequency $2\mu_s / (\hbar v)$, which decay

quadratically in x . Nevertheless, the Kondo cloud stays negative for all x . The oscillations can be interpreted as the impact of Friedel oscillations on the Kondo cloud. While Friedel oscillations in helical liquids are suppressed in the presence of ordinary scatterers, the spin-flip scattering off the magnetic QD to the oppositely moving channel generates an interference of the wave functions in both channels.

Conclusions. We couple a magnetic QD with spin $\frac{1}{2}$ to two helical liquids at the edges of a quantum spin Hall insulator. For the two channel Kondo model, we calculate the Toulouse points at which the Hamiltonian is mapped to a quadratic one. In contrast to non-interacting leads, the Toulouse points cover all possible coupling parameters to the QD at the cost of restricting the interaction strengths and Fermi velocity of the helical liquids. The Toulouse points separate into two qualitatively different sets. The first is related to the known Toulouse points of the non-interacting case. The second appears exclusively in the case of interactions. We determine the local screening and the Kondo screening cloud and calculate the signature of applied voltages.

We thank P. Simon and G. Zaránd for interesting discussions as well as the DFG, the Humboldt Foundation, and the ESF for financial support.

-
- [1] J. Kondo, *Progress of Theoretical Physics* **32**, 37 ff. (1964).
 - [2] A. C. Hewson, *The Kondo Problem To Heavy Fermions* (Cambridge University Press, 1993).
 - [3] E. Müller-Hartmann and J. Zittartz, *Phys. Rev. Lett.* **26**, 428 (1971).
 - [4] A. J. Leggett, S. Chakravarty, A. T. Dorsey, M. P. A. Fisher, A. Garg, and W. Zwerger, *Rev. Mod. Phys.* **59**,

- 1 (1987).
- [5] J. Martinek, Y. Utsumi, H. Imamura, J. Barnaś, S. Maekawa, J. König, and G. Schön, *Phys. Rev. Lett.* **91**, 127203 (2003).
- [6] A. Furusaki and N. Nagaosa, *Phys. Rev. Lett.* **72**, 892 (1994).
- [7] J. Maciejko, C. Liu, Y. Oreg, X.-L. Qi, C. Wu, and S.-C. Zhang, *Phys. Rev. Lett.* **102**, 256803 (2009).
- [8] L. Borda, *Phys. Rev. B* **75**, 041307 (2007).
- [9] I. Affleck and P. Simon, *Phys. Rev. Lett.* **86**, 2854 (2001).
- [10] C. L. Kane and E. J. Mele, *Phys. Rev. Lett.* **95**, 226801 (2005).
- [11] B. A. Bernevig, T. L. Hughes, and S.-C. Zhang, *Science* **314**, 1757 (2006).
- [12] C. Wu, B. A. Bernevig, and S.-C. Zhang, *Phys. Rev. Lett.* **96**, 106401 (2006).
- [13] M. Koenig, S. Wiedmann, C. Bruene, A. Roth, H. Buhmann, L. W. Molenkamp, X.-L. Qi, and S.-C. Zhang, *Science* **318**, 766 (2007).
- [14] M. Z. Hasan and C. L. Kane, *Reviews of Modern Physics* **82**, 3045 (2010).
- [15] Y. Tanaka, A. Furusaki, and K. A. Matveev, *Phys. Rev. Lett.* **106**, 236402 (2011).
- [16] P. Nozieres and A. Blandin, *Journal de Physique* **41**, 193 (1980).
- [17] K. T. Law, C. Y. Seng, P. A. Lee, and T. K. Ng, *Phys. Rev. B* **81**, 041305 (2010).
- [18] V. J. Emery and S. Kivelson, *Phys. Rev. B* **46**, 10812 (1992).
- [19] B. A. Bernevig, T. L. Hughes, and S.-C. Zhang, *Science* **314**, 1757 (2006).
- [20] J. von Delft and H. Schoeller, *Annalen der Physik* **7**, 225 (1998).
- [21] A. Schiller and S. Hershfield, *Phys. Rev. B* **58**, 14978 (1998).
- [22] G. Toulouse, *Phys. Rev. B* **2**, 270 (1970).
- [23] G. Zaránd and J. von Delft, *Phys. Rev. B* **61**, 6918 (2000).
- [24] J. Maciejko, *Phys. Rev. B* **85**, 245108 (2012).
- [25] Y. Nagaoka, *Phys. Rev.* **138**, A1112 (1965).